GEOPHYSICS, VOL. 71, NO. 3 (MAY-JUNE 2006); P. N33–N40, 9 FIGS., 1 TABLE.
10.1190/1.2195989

Determining capillary-pressure curve, pore-size distribution, and permeability from induced polarization of shaley sand

Maosong Tong[1], Li Li[2], Weinan Wang[1], and Yizhong Jiang[1]

ABSTRACT

An appropriate form of induced polarization (IP) acts as a bridge between the structure of a water-saturated core plug and its transport properties. The induced-polarization decay curves of natural rocks can be modeled as a weighted superposition of exponential relaxations. A singular-value decomposition method makes it possible to transform the induced-polarization decay data of the shaley sands into *relaxation-time spectrum*, defined as plot of weight versus the relaxation-time constant. We measured the induced-polarization decay curves of core samples from a formation of Daqing oil field using a four-electrode method. The decay curves were transformed to relaxation-time spectra that were used to estimate the capillary-pressure curves, the pore-size distribution, and the permeability of the shaley sands. The results show that salinity ranges from 1g/liter to 20 g/liter have little effect on the IP relaxation-time spectra. A pseudocapillary pressure curve can be derived from the IP relaxation-time spectrum by matching the pseudocapillary curve with that from HgAir. The best-matching coefficients of the studied cores change slightly for the samples. Defined as the value of pressure at which the injected mercury saturation is 5%, entry pressures of the cores can be estimated well from IP-derived capillary-pressure curves. Pore-size distributions generated from induced polarization and mercury capillary-pressure curves are comparable. Permeability can be predicted from IP measurements in the form of $K_{IP} = c \cdot T^m \cdot \phi^n$, where K_{IP} is the estimated permeability from IP relaxation spectrum in millidarcies (md), ϕ is the porosity in percentage, and T is average time constant of IP relaxation-time spectra in millis (ms). The constants and exponents from various rock formations are slightly different.

INTRODUCTION

The capillary-pressure curve, pore-size distribution, and permeability of rocks are of great importance for the general understanding of dynamic processes that involve fluid flow in the earth's crust. They are also needed in a number of applied fields such as the exploration and production of hydrocarbons, environmental and hydrogeologic studies, the utilization of hydrothermal energy, and underground storage. The distribution of pore neck (or throats) is an important characteristic of reservoir rock because it determines the magnitude of capillary pressures in a rock, and thus, the saturation-height profile, among other things.

At present, the most often-used method to determine the pore-size distribution, capillary-pressure curve, and permeability of a formation is to take cores from the formation during the drilling of the well and then to analyze the core plugs in a laboratory. Although the method has high precision, it is very expensive and the results may not be a good representation of the formation as a whole, because core plugs are small and discrete samples. On the other hand, testing cores under in situ conditions is extremely difficult. Thus, the possibility to measure accurately in situ capillary-pressure curve, pore-size distribution, and permeability by using borehole-geophysical logs is appealing.

One reliable logging method for determining capillary-pressure curve, pore-size distribution, and permeability is the use of the nuclear magnetic resonance (NMR) logging tool (Banavar and Schwartz, 1987; Gallegos and Smith, 1988; Baldwin and Yamanashi, 1991; Kleinberg, 1996; Balzarini et al., 1998; Volokitin et al., 1999; Fleury et al., 2001). The technique has several disadvantages: Among them are a small depth of investigation, high cost, and low signal-to-noise ratio (Weng, 2001). Because the internal structure of the pore space affects the electrolytic-charge transport

Manuscript received by the Editor March 11, 2005; revised manuscript received August 25, 2005; published online May 25, 2006.
[1]Daqing Petroleum Administrative Bureau, Well Logging Company, Research and Development Center, Daqing, Heilongjiang Province, People's Republic of China, 163412. E-mail: tongms@cj.dq.cnpc.com.cn; wangwn@cj.dq.cnpc.com.ca.
[2]Daqing Petroleum Institute, School of Chemistry and Chemical Engineering, Daqing, Heilongjiang Province, People's Republic of China, 163318. E-mail: lilytms@163.com.

and fluid flow in a similar way, the IP can be used as an in-situ permeability estimation method. It has several advantages compared to the NMR logging tools, including deep investigation area and high signal-to-noise ratio.

IP logging can be operated in frequency and time domain to estimate the hydraulic properties of shaley sands (Marshall and Madden, 1959; Barker, 1975; Vinegar and Waxman, 1984; Worthington and Collar, 1984; Börner et al., 1996; Lesmes and Morgan, 2001; Titov et al., 2002; Slater and Lesmes, 2002; Titov et al., 2004). In the frequency domain both the amplitude and the phase shift of the apparent impedance of the earth are measured at various frequencies. Theoretical models of IP response (Marshall and Madden, 1959; Titov et al., 2002) predict, and empirical evidence shows (Pelton et al., 1978) that there is a length scale to the impedance of current or that there is a relationship between grain size and frequency response. Sturrock et al. (1999) suggested that permeability estimation from frequency-domain IP can be improved by using the grain-size distribution as well as the specific surface.

The majority of models that quantify the relationship between the imaginary part of the conductivity and the hydraulic permeability use the grain-surface model with the Börner model (Börner et al., 1996) relating the imaginary conductivity to the surface area-to-porosity ratio (S_{por}) and to the formation factor (F). These are then used to estimate the hydraulic conductivity and cation-exchange capacity (CEC) of clays. Sturrock's model relies on the fact that there is a constant-phase angle (CPA) in the electrical response of rocks at different frequencies (Sturrock et al., 1999). Slater and Lesmes (2002) use a relationship to relate the imaginary part of conductivity to d_{10} (the diameter of the grain that is larger than 10% of the sample that presents as a linear relationship with hydraulic conductivity). Examples have been given by de Lima and Niwas (2000) to emphasize the combined use of electrical resistivity and induced-polarization measurement in computing hydraulic properties.

The time-domain IP for estimation of hydraulic properties has received much attention (Barker, 1975; Worthington and Collar, 1984; Titov et al., 2002). Chargeability was often used as the time-domain IP parameter. It is demonstrated that chargeability can be related smoothly and definitely to excess conductivity or intergranular permeability. The equation relating chargeability and permeability is nonunique because two values of permeability correspond to a given IP signal in all cases, except that of a maximum IP response (Worthington and Collar, 1984). On the other hand, the chargeability also relates to the formation water resistivity that changes greatly and is very difficult to obtain for water-flooded oil fields, such as Daqing Oil Field.

The IP decay curve contains much more information than chargeability, and it also relates to the geophysical properties of the water-bearing rock. In this paper, we estimate the capillary-pressure curve, pore-size distribution, and permeability from the IP decay curves of shaley sands.

EXPERIMENTAL PROCEDURE

The core samples selected for this study were cut from cores recovered from one shaley sand formation of Daqing Oil Field. Care has been taken to cover a wide range of parameter values. In this study the samples range from 5% to 26% in porosity and from 0.056×10^{-15} to 1584×10^{-15} m^2 in permeability. Porosities were determined using a helium porosimeter and the permeability was determined using steady-state gas-flow tests.

The IP decay curve was measured by a four-electrode system as shown in Figure 1. The sample holder was designed to apply simulated overburden stress to the sample. It is constructed entirely of polyformaldehyde to prevent metallic polarization. Electrical contact with the sample is made through the electrolyte solution that is maintained at the same concentration as that used in saturating the core. In Figure 1, A and B are the planar platinum (Pt) current electrodes. M and N are the nonpolarizing silver/silver chloride (Ag/AgCl) potential electrodes that are used to minimize the effects of electrode polarization that can occur at the fluid-electrode interface. The Ag/AgCl electrodes are positioned outside the current path to avoid further the additional polarization of the potential electrodes in the current path.

The data-acquisition system was a NI PCI-6070E card with a maximum sampling rate of 1.25 Mbit/s. The measurement sensitivity is 0.009 mV. The constant-current generator has an absolute error of 0.3 μA. The controlling unit has a switching time shorter than 1 μs and a drainage current less than 0.01 μA. The measurement was repeated four times and an average decay curve was obtained.

Laboratory measurements of induced polarization were made on cylindrical samples approximately 2.5 cm in length and 2.5 cm in diameter. Measurements were carried out at ambient laboratory temperatures, typically 25 ± 1°C. The current of 1 mA/cm^2 was applied on the samples for 120 s. The transient decay of the electrical potential as a function of time was measured for 120 s after the current was turned off.

Before the IP measurements, each sample was saturated with 5 g/liter NaCl brine, using the following procedure. Each sample was placed in a stainless-steel saturator, and the container was evacuated. The NaCl brine was then introduced under vacuum, followed by fluid pressurization up to 15 MPa to ensure complete saturation. The samples were left overnight under pressure. When the samples were removed from the saturator, gravimetric checks determined if complete saturation of the pore space had been achieved. This was carried out using the dry weight, pore volume, and brine density. All samples attained full-brine saturation.

In this study, we also investigate the effect of salinity on the spectra. The salinity was changed by soaking the sample in deionized water until the resistivity of the obtained water was consistently higher than 10^4 Ωm for two days. The sample, saturated with

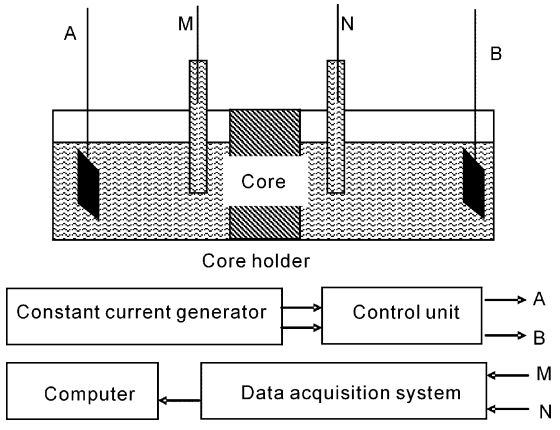

Figure 1. The experimental setup.

the fresh water, was dried in the oven at 80°C for 24 hours. Then it was checked to determine if the water was completely removed by the gravimetric method. The sample was subsequently saturated with NaCl brine of another concentration.

RELAXATION THEORY OF IP IN ROCK

A schematic of a pore contained within shaley sand is shown in Figure 2. The pore is spherical in shape with a radius R, and it has a plurality of pore throats with radius $r < R$, that enter the pore. The pore contains a series of clay-rich and clay-free zones. The induced-polarization method applies a substantially constant electric field to the formation in the direction shown in Figure 2. The clay-rich zones act as cation-selective membranes and restrict the flow of negatively charged cations under the electric field's influence. Thus, after sufficient time, an electrochemical gradient is established across the clay-free zones by the buildup of electrolyte concentration at the edge of the clay-rich zone.

Upon current termination, ions relax to equilibrium positions, and the concentration gradient decreases; which constitutes the induced-polarization decay curve. (Marshall and Madden, 1959; Vinegar and Waxman, 1984; Vinegar and Waxman, 1987; Vinegar and Waxman, 1988).

If the porous medium consisted of clay-free zones of all the same size, the induced-polarization decay curve would consist of a single, exponential decay of time constant T (Vinegar and Waxman, 1984; Vinegar and Waxman, 1987; Vinegar and Waxman, 1988).

$$T = \frac{L^2}{D}, \tag{1}$$

where D is the diffusion constant of electrolyte ions in the aqueous solution at formation temperature, and L is the relaxation distance of the clay-free zone along the direction of the applied electric field. The diffusion constant of electrolyte ions in the aqueous solution at formation temperature for NaCl solution at 25°C equals 1.5×10^{-8} cm^2/ms.

The clay-free relaxation distances are substantially the same as the pore-size distribution. The explanation for this is that the clay occurs naturally as a pore-lining material. In particular, the clay particles in the pore throat are the most effective membranes for the electrolyte contained in the pore (Figure 2). Thus, the scale of relaxation distances is substantially the same as the pore scale. So the following equation can be obtained:

$$R = \sqrt{DT}, \tag{2}$$

where R is the pore size in Figure 2. Because natural rocks contain a distribution of pore sizes, the IP-decay voltage $V(t)$ can be modeled as a weighted superposition of exponential relaxations. The moment that the applied electric field is terminated ($t = 0$), the voltage is $V(0)$. The normalized IP-decay signal $y(t) = V(t)/V(0)$ can then be represented by equation 3, where the distribution function $f(T)$ determines the magnitude of the relaxations and T_{min} and T_{max}, the smallest and largest relaxation-time constants, respectively, as follows:

$$y(t) = \frac{V(t)}{V(0)} = \int_{T_{\min}}^{T_{\max}} f(T)\exp\left(-\frac{t}{T}\right)dT, \tag{3}$$

where $f(T)$ is coefficient and T_{min} and T_{max} are the shortest- and the longest-time constants, respectively.

MULTIEXPONENTIAL INVERSION OF IP-RELAXATION DATA

Equation 3 is the first kind Fredholm linear integral equation (Weng, 2001). It can be recast as a least-squares minimization problem with nonnegativity constraint with

$$\Phi \equiv \|Mf - y\|^2 \rightarrow \min., M_{ij} \equiv \exp\left(-\frac{t_i}{T_j}\right) \tag{4}$$

subject to $f_i \geq 0$, where $y = (y_1, y_2, \ldots, y_m)^T$ is the IP decay signal, $f = (f_1, f_2, \ldots, f_n)^T$ is the amplitude of the component with relaxation time constant T_j, and T_j ($j = 1, 2, \ldots, n$) are the relaxation-time constants determined in advance. A typical, predefined relaxation-time constant T series, called *T arrangement*, is n points logarithmically selected from $T_{\min}$ to T_{max} in uniform steps. The amplitude of the component with relaxation f_i is a volume proportion of pore i in total pores of total pore volume in that the time constant equals T_i. The longest-time constant in the IP decay curve is contributed by those ions with the longest-relaxation distance. The curve of f versus T was called *induced-polarization relaxation-time spectrum*. The time constant relates to the pore size and the relaxation spectrum reflects the pore-size distribution of shaley sand (Vinegar and Waxman, 1987; Vinegar and Waxman, 1988). Once the distribution of the pore size is known, the formation permeability can be calculated approximately using different geometric models (Zhou et al., 2002).

It is impossible to solve equation 4 using Gaussian decomposition because the condition number of the matrix M is very high and can go up to the order of 10^{18} if we set the sampling interval at 0.1 ms and select 64 points logarithmically from 0.1 ms to 10 s in uniform steps. However, we can easily get the least-squares solution if we use the singular value decomposition (SVD) method for calculating M

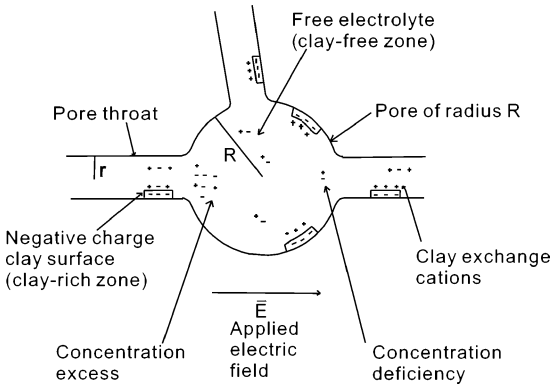

Figure 2. An idealized pore in a shaley sand and the charges carried by clay counterions and by sodium and chloride ions in the free electrolyte.

$$M_{m\times n} = U_{m\times n} \times W_{n\times n} \times V^T_{n\times n}, \quad (5)$$

where $U_{m\times n}$ is an orthogonal matrix with columns that are eigenvectors of $M \times M^T$, $V_{n\times n}$ is an orthogonal matrix with columns that are eigenvectors of $M^T \times M$, $W \equiv \lfloor diag(w_j) \rfloor_{n\times n}$ is a nonnegative diagonal matrix, and $w_j (1 \le j \le n)$ are the singular values of M. By convention, the ordering of the singular vectors is determined by high-to-low sorting of singular values, with the highest singular value in the upper-left index of W. Furthermore, $w_k > 0$ for $1 \le k \le r$, and $w_i = 0$ for $(r + 1) \le k \le n$, where r is the rank of M.

The resulting inverse solution is

$$\hat{f} = V \times \left[diag\left(\frac{1}{w_1}, \frac{1}{w_2}, \ldots, \frac{1}{w_r}, 0, \ldots, 0 \right) \right] \times (U^T \times y). \quad (6)$$

It is possible to obtain negative terms when inverting for the amplitudes of the relaxation time spectrum which is not physically meaningful. Therefore, a nonnegative restriction, i.e., $f_i \ge 0$ ($j = 1,2, \ldots, n$) must be added when we solve for the model (Prammer, 1994; Weng, 2001) using the following steps: (1) Starting with a full matrix M, a tentative solution f is computed. (2) If all components are nonnegative, the solution f is accepted. Otherwise, the column of M corresponding to the least amplitude is eliminated and a reduced matrix M' is obtained. At the same time the corresponding component in f is set to zero and also eliminated to form a reduced vector f'. (3) $M \Rightarrow M'$, so go back to step 1.

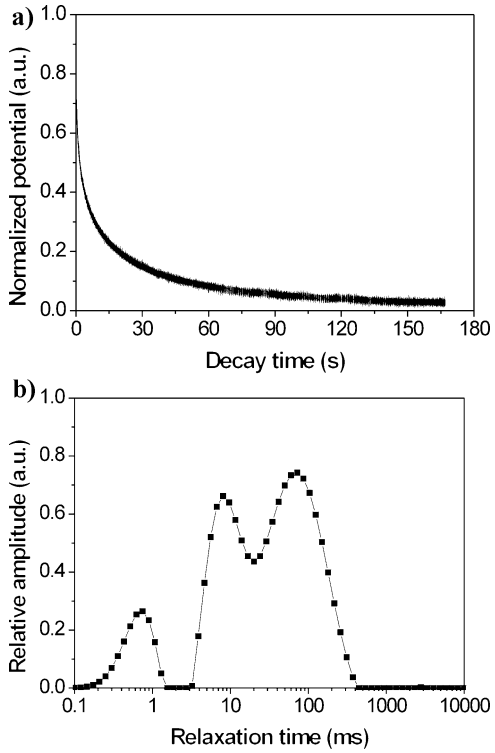

Figure 3. A measured IP decay curve and the corresponding relaxation-time spectrum. (a) Normalized decay curve and (b) relaxation-time spectrum (a.u. means arbitrary unit).

We repeat the above steps until all components of f are greater than or equal to zero. A typical measured IP decay curve and the inversed-relaxation spectrum are shown in Figure 3a and 3b, respectively. Figure 3b shows that the relaxation spectrum is very smooth and shows a multipeak characteristic.

HYDRAULIC PROPERTIES FROM INDUCED-POLARIZATION RELAXATION TIME SPECTRA

Capillary-pressure curves from IP

A capillary-pressure curve describes the injection of a nonwetting fluid into a porous medium (rock). More precisely, every point of such a curve shows the percentage of the pore space occupied by a nonwetting fluid when a certain overpressure is applied to this fluid. The pressure at which a fluid enters a pore is determined by the surface tension of the fluid interface and the radius of a pore's neck, expressed as

$$P_c = \frac{2\sigma \cos\theta}{r}, \quad (7)$$

where σ is the surface tension, θ is the contact angle between the nonwetting fluid interface and the pore wall, r is the pore throat radius in cm, and P_c is the capillary pressure in dynes/cm^2. For the mercury air system:

$$r = \frac{0.75}{P_c}. \quad (8)$$

Using this equation, the pore-throat radius can be estimated from the pressure distributions.

Both IP relaxation-time spectrum and capillary-pressure measurements represent the distributions of pore volumes that correspond to a certain pore radius ($\sim\sqrt{T}$) or a certain pore-throat radius ($\sim 1/P_c$). The method of converting IP relaxation-time spectra to capillary-pressure curves requires the existence of a relationship between the radii of pore and pore-throats. One can assume that pore-throat radius and pore radius may be directly proportional to one another. Using equation 1 we obtain

$$r = \frac{R}{C} = \frac{\sqrt{DT}}{C}, \quad (9)$$

where C is the constant relating pore radius to pore-throat radius.

Using equations 8 and 9, we obtain

$$P_c = \frac{0.75C}{\sqrt{D}} T^{-1/2} = kT^{-1/2}, \quad (10)$$

where $k = 0.75C/\sqrt{D}$ is a constant relating capillary pressure to IP relaxation time.

To arrive at a capillary-pressure curve starting from IP relaxation spectrum, one must: (1) Sum the amplitudes from the shortest- to the longest-time constant to obtain a cumulative curve with an axis of time constant. For each time constant, the corresponding y-axis value is the sum of its amplitude and that of all the time constants with less value than it. (2) Plot the curve on $T^{-1/2}$ scale. (3) Interchange the x- and y-axes of the plot. (4) Rescale with proportional-

ity constant k. In our study, we find an optimum k value by making the best match between the capillary curves from HgAir and IP.

Another important capillary-pressure curve parameter is the entry pressure (PcEntry). The entry pressure is the capillary pressure when the nonwetting phase begins to enter the pore space. Knowing the entry pressure is noteworthy, for example, in such problems as predicting the sealing rock strength or looking at the difference between the free water level and hydrocarbon-water contact. Since pore-neck distribution is related to pore-size distribution, it is clear that the possibility exists to predict PcEntry from the IP relaxation-time spectrum. The PcEntry is, of course, related to the largest present pore-neck size. In this paper, *PcEntry* is defined as the value of P_c when the injected mercury saturation is $S_{Hg} = 5\%$.

Pore-size distributions from IP

Because fluid flow is controlled by the narrowest connections between void space, capillary-pressure tests provide information about the pore throats of the total porosity network. A distribution curve can be derived relating pore volume to mean throat diameter.

As mentioned above, equation 10 shows that the pore-throat size is proportional to the root of relaxation time. Thus, the pore-throat-size distribution can be obtained from the relaxation spectrum.

Predicting permeability

One of our major objectives was to investigate the relationship between permeability and IP measurements, as well as to improve our understanding of permeability estimates from IP measurements.

Several empirical relations have shown how permeability K depends on porosity and pore distribution. A simplest relation is in the form of

$$K \cong \langle \overline{R^2} \rangle, \tag{11}$$

where K is the permeability in millidarcies and $\langle \overline{R^2} \rangle$ is the mean-square pore radius in square microns that can be determined from the pore-size distribution. A more accurate empirical relation is (Vinegar and Waxman, 1987; Vinegar and Waxman, 1988)

$$K \cong c\phi^m \langle \overline{R^2} \rangle, \tag{12}$$

where c and m are constants and ϕ is porosity. As shown in equation 2, square-pore radius is proportional to IP relaxation-time constant. So we develop a new model that includes the porosity and the average relaxation-time constant with

$$K_{IP} = c \cdot T^m \cdot \phi^n, \tag{13}$$

where K_{IP} is the estimated permeability from IP relaxation spectrum in millidarcies (1 md = 10^{-15} m^2); c, m, and n are constants; ϕ is the porosity in percentage; and T is the average IP relaxation-time constant in millis.

To study the correlations among groups of properties, K, T, and ϕ, we looked for the value of free parameters that minimized the mean-squared logarithmic error of fit using

$$\varepsilon^2 = \frac{1}{N}\sum_{i=1}^{N} [\ln K_m(i) - \ln K_{IP}(i)]^2 \quad \delta = e^{\varepsilon}, \tag{14}$$

where N is the number of samples; $K_m(i)$ and $K_{IP}(i)$ are the measured and estimated permeabilities of the sample i, respectively; and δ is the error factor. The constants of c, m, and n in equation 13 are chosen to minimize ε^2.

In this study, we use two average time constants, i.e., geometric-mean-time constant T_g and arithmetic-mean-time constant T_a, that are defined as follows, respectively:

$$T_g = \left(\prod_{i=1}^{N} T_i^{f_i} \right)^{\frac{1}{\sum_{i=1}^{N} f_i}} \tag{15}$$

and

$$T_a = \frac{\sum_{i=1}^{N} f_i \times T_i}{\sum_{i=1}^{N} f_i}. \tag{16}$$

Therefore, equation 13 can be rewritten as

$$K_{IP(T_g)} = cT_g^m \phi^n \tag{17}$$

and

$$K_{IP(T_a)} = cT_a^m \phi^n. \tag{18}$$

RESULTS AND DISCUSSION

Figure 4 shows the spectra of samples saturated with NaCl solution of different salinity. It can be seen that the salinity has a small influence on the relaxation in the solution concentration range from 1 g/liter to 20g/liter. The salinity only affects the excess-ion concentration and deficiency-ion concentration under the applied elec-

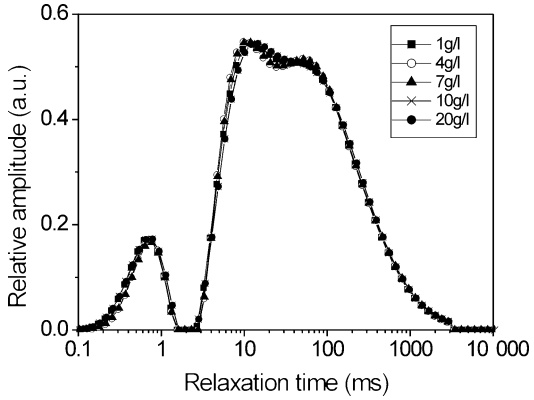

Figure 4. The IP relaxation-time spectra of one core, saturated with NaCl electrolyte with different salinity (a.u. means arbitrary unit).

tric field and then it affects the value of the time-domain IP decay voltage. In our inversion of the relaxation-time spectra, we used the normalized IP-decay signal $y(t) = V(t)/V(0)$. On the other hand, the diffusion constant changes very slightly in the salinity range from 1 g/liter to 20 g/liter. Thus, the normalized IP decay signal is also the same for different salinity.

Figure 5 shows the capillary-pressure curves from HgAir and IP of two cores. It is shown that the two curves superpose well for each sample. Note that the constant k may vary with the cores from different formations. In our study, 55 cores are from one formation. One can see from Table 1 that k ranges from 1.53 to 3.12. Because C is the constant relating pore radius to pore-throat radius, it changes little for one formation. On the other hand, D is a constant at the experimental temperature, so k changes a little. Before IP logging, the k values for different formations can be obtained from core analysis. This result allows us to use the IP relaxation-time spectra to determine the capillary-pressure curves.

The crosses in Figure 6 show the well correlations for 55 cores, where values of k were chosen specially to minimize the difference between capillary-pressure values of HgAir and IP for each plug discussed above. The correlation coefficient of the crossplot is 0.92.

Figure 7 shows the pore-size distribution of two cores from IP relaxation spectra and HgAir. Sample (a) has one population of pore size ranging from 0.1 μm to 4 μm. It can be seen that the pore-size distribution from IP is in good agreement with that from HgAir. Sample (b) has two peaks in the pore-throat size distribution (Figure 7b), and the one from the IP also has two peaks. Their shapes are very similar. These results indicate that the IP relaxation spectrum reflects the pore-size distribution directly.

We have studied estimators of permeability in the form of equation 17 for one set of data (102 samples) using

$$K_{IP(T_g)} = 2.5 \times 10^{-10} \times T_g^{1.12}\phi^{3.78}, \quad \delta = 1.94. \quad (19)$$

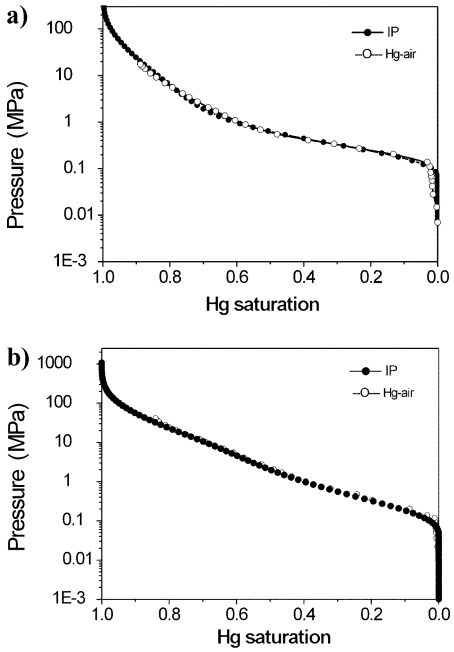

Figure 5. HgAir capillary curves compared with IP-derived capillary curves for two samples: (a) $K = 0.075$ md, $\phi = 10.91\%$ and (b) $K = 2.82$ md, $\phi = 15.78\%$.

The results in Figure 8 show that the permeability can be predicated from the IP relaxation-time spectra combined with the porosity data of the samples. For another formation of Daqing Oil Field, the result relation is

Table 1. Characteristics of samples.

Sample number	φ %	K $\times 10^{-15}$ m^2	k $\times 10^4$ ms$^{1/2}$/cm	Sample number	φ %	K $\times 10^{-15}$ m^2	k $\times 10^4$ ms$^{1/2}$/cm
1	9.4	0.0056	2.13	29	15.3	4.46	2.33
2	12.1	0.079	1.78	30	11.6	5.01	1.78
3	8.9	0.089	2.17	31	11.8	7.07	2.87
4	9.6	0.100	1.54	32	21.62	7.94	1.96
5	13.2	0.112	2.31	33	18.20	8.91	2.11
6	6.5	0.126	2.07	34	6.96	15.80	1.75
7	6.8	0.141	2.44	35	17.35	19.90	2.51
8	10.2	0.15	1.75	36	23.90	39.81	1.57
9	12.8	0.17	2.12	37	21.00	44.60	1.59
10	13.8	0.20	1.64	38	25.30	70.79	2.05
11	9.3	0.36	1.53	39	15.81	79.43	2.19
12	6.9	0.35	1.63	40	21.00	125.80	1.75
13	15.2	0.39	1.94	41	12.50	177.80	1.81
14	7.9	0.44	2.02	42	23.80	199.50	2.71
15	5.0	0.50	1.91	43	24.20	223.80	1.61
16	15.6	0.52	1.67	44	16.36	281.80	2.28
17	7.6	0.63	3.12	45	13.81	316.20	2.17
18	12.1	1.25	2.15	46	17.98	354.80	1.58
19	12.8	1.41	2.01	47	19.30	446.60	1.81
20	6.9	1.58	1.73	48	19.50	501.10	1.82
21	15.3	1.77	1.84	49	25.37	562.30	2.35
22	12.6	1.99	1.58	50	26.00	630.90	1.55
23	15.9	2.23	1.77	51	25.36	707.90	2.21
24	12.5	2.51	2.22	52	18.90	891.20	2.32
25	8.9	2.81	2.17	53	16.39	1122.40	2.05
26	9.4	3.16	2.13	54	23.58	1412.50	2.75
27	12.1	3.54	2.06	55	25.69	1584.00	1.95
28	8.9	3.98	2.07	—	—	—	—

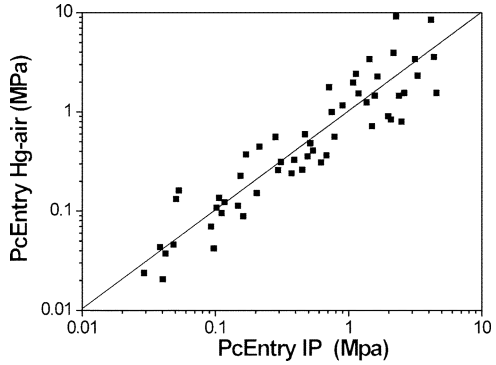

Figure 6. Crossplots of values of PcEntry as found from HgAir capillary curves versus those calculated from IP relaxation-time spectrum.

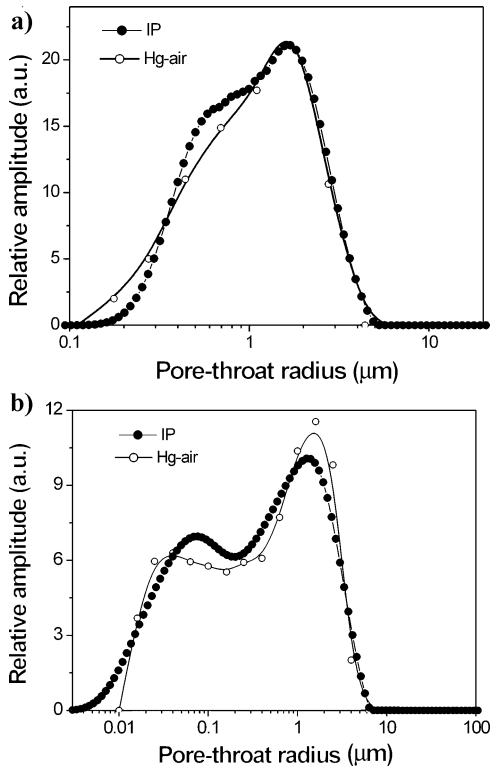

Figure 7. The pore-size distributions from the capillary-pressure curve and IP-relaxation spectra (a.u. means arbitrary unit). (a) K = 0.075 md, ϕ = 10.91% and (b) K = 2.82 md, ϕ = 15.78%.

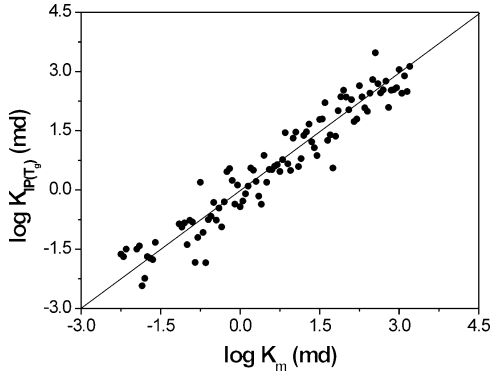

Figure 8. Log-permeability estimated from equation 15 versus log permeability by conventional measurement. T_g is the geometric-mean relaxation-time constant.

$$K_{IP(T_g)} = 2.41 \times 10^{-10} \times T_g^{1.16}\phi^{3.65}, \quad \delta = 2.28. \quad (20)$$

We also have studied estimators of permeability in the form of equation 18. Similar results can be obtained with T_a. For the data (102 samples) used in equation 19

$$K_{IP(T_a)} = 7.5 \times 10^{-11} \times T_a^{1.03}\phi^{4.14}, \quad \delta = 2.18. \quad (21)$$

Figure 9 shows the scatter graph of K_m verses $K_{IP(T_a)}$. The narrow spread of the data confirms the goodness of this estimator (equation 18). For the cores used in equation 21, the result relation is

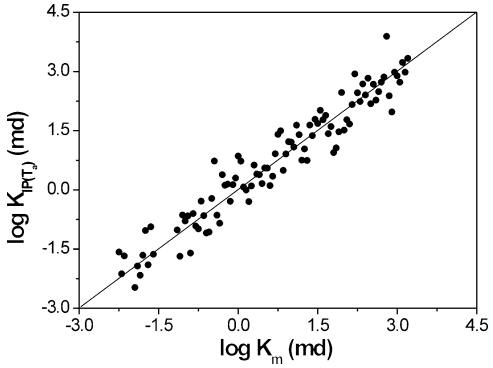

Figure 9. Log permeability estimated from equation 16 versus log permeability by conventional measurement. T_a is the arithmetic-mean time constant.

$$K_{IP(T_a)} = 7.3 \times 10^{-11} \times T_a^{1.08}\phi^{3.98}, \quad \delta = 2.32. \quad (22)$$

These results show that the constants and exponents in equations 17 and 18 are different, for each formation. We also can see that these differences are small. Before using the permeability estimation models in the downhole, these constants and exponents should be obtained from experimental studies of core samples from the reservoirs.

CONCLUSIONS

Smooth and continuous relaxation-time spectra can be inversed by using the singular-value decomposition algorithm. The results show that the salinity ranges from 1 g/liter to 20 g/liter have little effect on the IP relaxation-time spectra. Capillary-pressure curves can be obtained accurately from IP relaxation spectra, and the entry pressures of the cores can be estimated well from IP-derived capillary-pressure curves. Since IP measurements are fast, cheap, and nondestructive, this offers an attractive alternative to conventional capillary-pressure measurements. It should be noted that the constant $k = 0.75C/\sqrt{D}$ may vary with the cores from different formations but it changes little within one formation. In our study, it ranges from 1.53 to 3.12.

An accurate pore-size distribution (relaxation time) can be obtained from core IP measurement. The IP relaxation-time distribution correlates well with pore-size distribution derived from capillary-pressure measurements.

Our data clearly indicate that IP measurements greatly improve statistical significance of permeability correlations. Good estimations of permeability are obtained using IP in the form of $K_{IP(T_g)} = cT_g^m\phi^n$ or $K_{IP(T_a)} = c \cdot T_a^m \cdot \phi^n$. The constants and exponents vary lightly with formations.

ACKNOWLEDGMENTS

The work was supported by the Postdoctoral Research Project of Daqing Oil Field and the Major Project of Daqing Petroleum Administrative Bureau (No.DQKJZB200318).

REFERENCES

Baldwin, B. A., and W. S. Yamanashi, 1991, Capillary-pressure determination from NMR images of centrifuged core plugs, Berea Sandstones: The

Log Analyst, **32**, 550–556.
Balzarini, M., A. Brancolini, and P. Gossenberg, 1998, Permeability estimation from NMR diffusion measurements in reservoir rocks: Journal of Magnetic Resonance Imaging, **16**, 601–603.
Banavar, J. R., and L. M. Schwartz, 1987, Magnetic resonance as a probe of permeability in porous media: Physical Review Letters, **58**, 1411–1414.
Barker, R. D., 1975, A note on the induced polarization of the Bunter sandstone: Geoexploration, **13**, 227–233.
Börner, F. D., J. R. Schopper, and A. Weller, 1996, Evaluation of transport and storage properties in the soil and groundwater zone from induced polarization measurements: Geophysical Prospecting, **44**, 583–602.
de Lima, O. A. L., and S. Niwas, 2000, Estimation of hydraulic parameters of shaley sandstone aquifers from geoelectrical measurements: Journal of Hydrology, **235**, 12–26.
Fleury, M., F. Deflandre, and S. Godefroy, 2001, Validity of permeability prediction from NMR measurements: Comptes Rendus de l'Academie des Sciences Series IIC Chemistry, **4**, 869–872.
Gallegos, D. P., and D. M. Smith, 1988, A NMR technique for the analysis of pore structure: determination of continuous pore-size distributions: Journal of Geotechnical and Geoenvironmental Engineering, **122**, 143–153.
Kleinberg, R. L., 1996, Utility of NMR T_2 distributions, connection with capillary pressure, clay effect, and determination of the surface relaxivity parameter ρ_2: Journal of Magnetic Resonance Imaging, **14**, 761–767.
Lesmes, D. P., and F. D. Morgan, 2001, Dielectric spectroscopy of sedimentary rocks: Journal of Geophysical Research, **106**, 13329–13346.
Marshall, D. J., and T. R. Madden, 1959, Induced polarization, a study of its causes: Geophysics, **24**, 790–816.
Pelton, W. H., S. H. Ward, P. G. Hallof, W. R. Sill, and P. H. Nelson, 1978, Mineral discrimination and removal of inductive coupling with multifrequency IP: Geophysics, **43**, 588–609.
Prammer, M. G., 1994, NMR pore-size distributions and permeability at the well site: Society of Petroleum Engineers, Paper 28368.
Slater, L., and D. P. Lesmes, 2002, Electrical-hydraulic relationships observed for unconsolidated sediments: Water Resources Research, **38**, 31–1–31–10.
Sturrock, J. T., D. Lesmes, and F. D. Morgan, 1999, Permeability estimation using spectral induced polarization measurements: Proceedings of the Symposium on the Application of Geophysics to Engineering and Environmental Problems, Environmental and Engineering Geophysical Society, 409–415.
Titov, K., A. Kemna, A. Tarasov, and H. Vereecken, 2004, Induced polarization of unsaturated sands determined through time domain measurements: Vadose Zone Journal **3**, 1160–1168.
Titov, K., V. Komarov, V. Tarasov, and A. Levitski, 2002, Theoretical and experimental study of time domain-induced polarization in water-saturated sands: Journal of Applied Geophysics, **50**, 417–433.
Vinegar, H. J., and M. H. Waxman, 1984, Induced polarization of shaley sands: Geophysics, **49**, 1267–1287.
Vinegar, H. J., and M. H. Waxman, 1987, In-situ method for determining pore-size distribution capillary pressure and permeability: U. S. Patent 4,644,283.
Vinegar, H. J., and M. H. Waxman, 1988, In-situ method for determining formation permeability: U. S. Patent 4,743,854.
Volokitin, Y., W. Looyestijn, W. Slijkerman, and J. Hofman, 1999, Constructing capillary-pressure curves from NMR log data in the pressing of hydrocarbons: The Society of Petrophysicists and Well Log Analysts, Paper KKK.
Weng, A., 2001, Study on data processing theories and experiments of NMR logging (in Chinese): Ph.D. thesis, Jilin University.
Worthington, P. F., and F. A. Collar, 1984, Relevance of induced polarization to quantitative formation evaluation: Marine and Petroleum Geology, **1**, 14–26.
Zhou, C., X. Chen, Z. Si, S. Li, and W. Gao, 2002, On permeability determination with NMR echo trains: Well Logging Technology (in Chinese), 26, 123–126.